Journal of Applied Physics

Magnetic and magneto-transport properties of Mn_4N thin films by Ni substitution and their possibility of magnetic compensation

Cite as: J. Appl. Phys. **125**, 213902 (2019); https://doi.org/10.1063/1.5089869
Submitted: 23 January 2019 . Accepted: 12 May 2019 . Published Online: 03 June 2019

Taro Komori, Toshiki Gushi, Akihito Anzai, Laurent Vila, Jean-Philippe Attané, Stefania Pizzini, Jan Vogel, Shinji Isogami, Kaoru Toko, and Takashi Suemasu

Journal of Applied Physics ARTICLE scitation.org/journal/jap

Magnetic and magneto-transport properties of Mn_4N thin films by Ni substitution and their possibility of magnetic compensation

Cite as: J. Appl. Phys. **125**, 213902 (2019); doi: 10.1063/1.5089869
Submitted: 23 January 2019 · Accepted: 12 May 2019 ·
Published Online: 3 June 2019

Taro Komori,[1] Toshiki Gushi,[1,2] Akihito Anzai,[1] Laurent Vila,[2] Jean-Philippe Attané,[2] Stefania Pizzini,[3] Jan Vogel,[3] Shinji Isogami,[4] Kaoru Toko,[1] and Takashi Suemasu[1,a)]

AFFILIATIONS

[1]Institute of Applied Physics, Graduate School of Pure and Applied Sciences, University of Tsukuba, Tsukuba, Ibaraki 305-8573, Japan
[2]Université Grenoble Alpes, CNRS, CEA, Grenoble INP, IRIG-SPINTEC, F-38000 Grenoble, France
[3]Institut Néel, CNRS/UGA, 25 avenue des Martyrs, F-38042 Grenoble, France
[4]Research Center for Magnetic and Spintronic Materials, National Institute for Materials Science (NIMS), Tsukuba 305-0047, Japan

[a)] **Author to whom correspondence should be addressed:** suemasu@bk.tsukuba.ac.jp

ABSTRACT

Ferrimagnets are of interest in spintronics owing to the enhancement of spin transfer and spin–orbit torque in the vicinity of the magnetic compensation point. Here, we study the possibility of achieving compensation at room temperature in $Mn_{4-x}Ni_xN$ films grown on $SrTiO_3$(001) substrates by molecular beam epitaxy. The magnetic and magneto-transport properties of 30-nm-thick epitaxial $Mn_{4-x}Ni_xN$ films ($x = 0$, 0.1, 0.25, and 0.5) were investigated. Ni introduction in Mn_4N causes the spontaneous magnetization (M_S) to decrease by 45% at $x = 0.1$ and by 75% at $x = 0.25$. All samples exhibited the perpendicular magnetic anisotropy required for spintronic applications as well as displaying a sharp magnetization reversal. Remarkably, the sign of the anomalous Hall resistivity changed in the samples between $x = 0.1$ and 0.25. Further, the magnetization increased for $x = 0$ and 0.1 and decreased for $x = 0.25$ when the temperature was decreased. Based on these results, we propose that there is a magnetic compensation composition between $x = 0.1$ and 0.25, where the magnetization of $Mn_{4-x}Ni_xN$ becomes zero at room temperature. The small M_S and perpendicular magnetic anisotropy of the $Mn_{4-x}Ni_xN$ thin films, thus, make them suitable candidates for use in spin transfer torque-based devices.

I. INTRODUCTION

The physics of spin torque is based on a transfer of angular momentum to the magnetization to induce its precession or to switch it. The flow of angular momentum is caused by spin-polarized current in the case of spin transfer torques[1,2] or arises from spin–orbit interactions, such as the spin Hall effect or the Edelstein–Rashba effect[3,4] in the case of spin–orbit torques. Magnetization switching is easier if the spontaneous magnetization of the magnetic element is small. This recently triggered a renewal of interest in ferrimagnets to develop fast, high-density, and nonvolatile memory devices, such as racetrack memory,[5,6] domain wall (DW) motion magnetoresistive random access memory,[7] or spin–orbit torques magnetoresistive random access memory. In particular, current-induced DW motion (CIDWM) is faster in antiferromagnetic[8,9] and ferrimagnetic[10,11] materials than in ferromagnetic materials.

To enhance the spin torques in ferrimagnetic materials, it is, thus, necessary to get close to the angular momentum compensation temperature (T_A), which can differ from the magnetic compensation temperature (T_M).[11,12] In rare-earth-based ferrimagnets, the idea is, thus, to perform the experiments at the compensation temperature T_A.[13] For instance, the DW velocity (v_{DW}) in a $Gd_{44}Co_{56}$ ferrimagnetic nanowire has been reported to reach a record value of 1.3 km/s close to T_A (260 K).[14] Moreover, many experiments and discussions have also been conducted on the operation of ferrimagnetic materials at T_A regarding other aspects such

as spin-wave emission,[15] Dzyaloshinskii–Moriya interaction,[16] and maximized exchange coupling torque.[17] In this context, we have paid special attention to ferrimagnetic Mn_4N, which is composed of abundant and inexpensive elements. Recent experiments have shown that epitaxial Mn_4N thin films exhibit a perpendicular magnetization, remarkable magnetic properties within particular millimetric and smooth DWs,[18] and record DW velocities owing to spin transfer torque.[19] As such, we have focused on ferrimagnetic Mn_4N doped with Ni to obtain a material close to magnetic compensation at room temperature (RT). Using neutron diffraction, the magnetic moment of the Mn atoms in bulk cubic Mn_4N was measured and it was found to be $3.53\,\mu_B$ at the corner sites (I sites) and $-0.89\,\mu_B$ at the face-centered sites (II sites),[20] as shown in Fig. 1, where μ_B is the Bohr magneton; the Mn atoms are denoted as Mn(I) and Mn(II), respectively. The easy magnetization axis of bulk Mn_4N is in the [111] direction.[21] In contrast, for thin films, the ratios of the perpendicular lattice constant c to the in-plane lattice constant a, c/a, were found to be ∼0.99, regardless of the lattice mismatch to various substrates,[22–24] and the samples exhibited perpendicular magnetic anisotropy (PMA) large enough to obtain an easy magnetization axis along the [001] direction. The uniaxial magnetic anisotropy constant (K_u) of Mn_4N thin films has been reported to be $\sim 10^5$ J/m^3.[25–28] Materials with PMA generally have Bloch DWs, which contribute to faster DW motion with small current.[28] The width of the DW (Δ) in the nanowire is given by Eq. (1),[29]

$$\Delta = \sqrt{\frac{A}{K_u}}, \tag{1}$$

where A is the exchange stiffness. As K_u increases, Δ decreases, leading to the reduction in the threshold current density (j_{th}) necessary to move the DWs. This behavior occurs because the energy required to cause a precession of magnetic moments in the DW is determined by the difference in energy between the Bloch and the Neel DWs, which is proportional to Δ.[28,30] In this respect, materials with PMA are advantageous for CIDWM devices. Furthermore, Mn_4N thin films have been reported to have a relatively small M_S of ∼100 kA/m.[20,25,26] The drift velocity $\boldsymbol{u}$ of DWs submitted to spin polarized currents is given by[31]

$$\boldsymbol{u} = \frac{Pg\mu_B}{2eM_S}\boldsymbol{J}, \tag{2}$$

where P is the spin polarization of the electrical conductivity, g is the g factor, e is the elemental charge, and $\boldsymbol{J}$ is the current density. When $|\boldsymbol{J}|$ is large, we can approximate v_{DW} to be close to $|\boldsymbol{u}|$. Because $|\boldsymbol{u}|$ is inversely proportional to M_S, a smaller M_S should produce faster DW motion and a lower threshold current.[10] Small values of M_S have been reported for Mn_4N thin films grown on glass,[32] Si(001),[33] MgO(001),[22,24,26,34,35] and $SrTiO_3$ (STO)(001)[22,23] substrates. Indeed, we achieved a v_{DW} of 900 m/s at $j = 1.2 \times 10^{12}$ A/m^2 for a Mn_4N nanowire grown on STO(001) without applying an external magnetic field.[19]

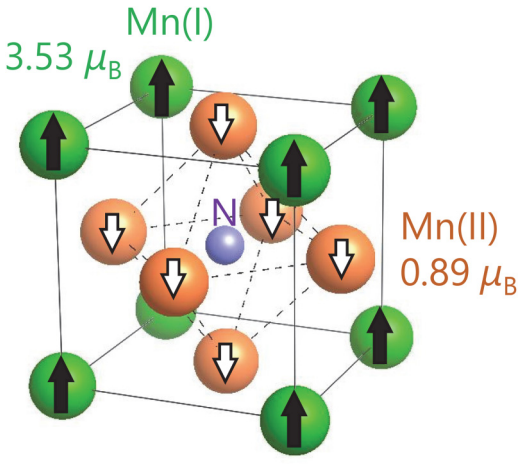

FIG. 1. Crystal structure of antiperovskite-type Mn_4N. The magnetic moment of corner-site Mn atoms, Mn(I), is antiparallel to that of face-centered Mn atoms, Mn(II).

Substituting other transition metal atoms for Mn atoms in Mn_4N is an effective way of modifying the material's magnetic properties. In previous studies, we grew $Co_xMn_{4-x}N$[23] and $Fe_{4-x}Mn_xN$[26] epitaxial thin films by molecular beam epitaxy (MBE) and investigated their crystalline qualities and magnetic properties. The M_S of these materials changed depending on their composition.[23,26,36] In contrast to what we predicted, however, the M_S and PMA were drastically decreased in the $Mn_{4-x}Ni_xN$ epitaxial thin films on MgO(001), even when only a small amount of Ni was introduced.[27] The M_S decreased remarkably from 86.3 kA/m (Mn_4N, $x = 0$) to 24.2 kA/m ($x = 0.1$) and then to 19.0 kA/m ($x = 0.25$) at RT. At $x > 0.25$, the PMA vanished. Therefore, much faster v_{DW} can be expected in $Mn_{4-x}Ni_xN$ at RT when it is close to the magnetic compensation point.

In the current study, we grew $Mn_{4-x}Ni_xN$ ($x = 0$, 0.1, 0.25, and 0.5) epitaxial thin films on STO(001), which has a far smaller lattice mismatch to Mn_4N (−0.4%) than to MgO(001) (−7.6%), and investigated their crystalline qualities and magnetic and magneto-transport properties, which we compared with those of the samples deposited on MgO(001). We also discuss the possibility of magnetic compensation in $Mn_{4-x}Ni_xN$ at RT to assess the use of $Mn_{4-x}Ni_xN$ thin films in spintronic devices.

II. METHODS

A. Preparation of $Mn_{4-x}Ni_xN$ thin films

$Mn_{4-x}Ni_xN$ ($x = 0$, 0.1, 0.25, and 0.5) thin films were grown on STO(001) substrates in an MBE setup equipped with conventional Knudsen cells for solid sources of Mn and Ni and radio-frequency nitrogen plasma. We chose STO(001) because of its excellent lattice match to Mn_4N, the higher degree of crystal orientation of Mn_4N epitaxial films on STO(001) along the c-axis compared with on MgO (001), and its extraordinarily large magnetic domains (over 1 mm in size).[18] To prepare the STO(001) substrates, we washed them with organic solvents and water and then cleaned them with buffered hydrofluoric acid. This process greatly reduced the surface roughness (the resultant root-mean-squared roughness was 0.2 − 0.8 nm) and formed a stepped surface for epitaxial growth.[37] The deposition rates of Mn and Ni were independently measured and controlled by

TABLE I. Thicknesses of $Mn_{4-x}Ni_xN$ and SiO_2 capping layers.

X	t_{sample} (nm)	t_{cap} (nm)
0	23.80	3.28
0.1	24.46	3.41
0.25	25.12	3.55
0.5	34.3	2.2

changing the crucible temperature of each Knudsen cell. The calculation was performed by assuming that these rates would not change even if the materials were deposited simultaneously. We set the substrate temperature (T_S) during growth at 450 °C.[27] Because the vapor pressures of Mn and Ni are sufficiently low at $T_S = 450$ °C, re-evaporation of these elements from the substrate was negligible. The radio-frequency plasma power was set at 108 W, and the flow rate of N_2 was set at ~1.0 sccm so that the emission intensity at a wavelength of 336 nm would be around 2900 counts at the spectrometer (QE Pro, Ocean Optics Inc., USA). An approximately 3-nm-thick SiO_2 capping layer was sputtered onto each sample. Table I summarizes the sample preparation details. The thicknesses of the grown layers were measured by X-ray reflectivity.

B. Evaluation of $Mn_{4-x}Ni_xN$ thin films

The crystalline qualities of the samples were evaluated by reflection high-energy electron diffraction (RHEED), out-of-plane (ω–2θ) X-ray diffraction (XRD), and in-plane (ϕ–$2\theta_\chi$) XRD (Smart Lab, Rigaku Inc, Japan). A Cu-Kα radiation source was used for XRD, and Ge(220) single crystals were set to monochromatize the X-ray beam. The magnetization vs magnetic field (M–H) loops were measured at RT by a vibrating sample magnetometer (VSM) using $6 \times 6\ mm^2$ samples. K_u and the effective magnetic anisotropy constant (K_u^{eff}) were calculated from the following equations:

$$K_u = K_u^{eff} + \frac{\mu_0}{2} M_S^2, \tag{3}$$

$$K_u^{eff} = \left(\mu_0 \int_0^{M_S} H\, dm\right)_{hard} - \left(\mu_0 \int_0^{M_S} H\, dm\right)_{easy}, \tag{4}$$

where easy (hard) refers to the easy (hard) magnetization axis. The $\mu_0 M_S^2/2$ term in Eq. (3) is the demagnetization component.[38] Because the magnetization could not be saturated when the field was applied in the VSM along the hard axis, it was impossible to correctly calculate these constants from the measured M–H loops. Thus, we used the fact that the loops acquired from the anomalous Hall effect (AHE) measurements (mentioned later) correspond to the M–H loops measured by VSM. We calculated the subtractions of the loops from the AHE using Eqs. (3) and (4).[39] Additionally, since the Hall voltage is known to be proportional to $M_\perp/M_S$, we calculated $M_{||}$ using Eq. (5), assuming that the layer is well squared.

$$M_{||} = M_S \sqrt{1 - \left(\frac{M_\perp}{M_S}\right)^2}. \tag{5}$$

Here, $M_{||}$ ($M_\perp$) is the in-plane (vertical) component of the magnetization. The temperature dependence of the magnetization was measured using a VSM-superconducting quantum interference device (Quantum Design). The field was set to 0.1 T perpendicular to the plane, and the temperature was modulated from 5 to 350 K under field cooling.

AHE measurements were performed with a physical properties measurement system (Quantum Design). To clarify the effect of the substrate, we also characterized $Mn_{4-x}Ni_xN$ ($x = 0$, 0.1, 0.25, and 0.5) epitaxial thin films grown on MgO(001). The growth of $Mn_{4-x}Ni_xN$ epitaxial films on MgO(001) and their magnetic properties has been reported in Ref. 27. We used the Van der Pauw method for the AHE measurements, as shown in the inset of Fig. 4(a). The magnetic field was applied from −3 to 3 T perpendicular to the plane and from −9 to 9 T in the in-plane direction.

III. RESULTS AND DISCUSSION

A. Crystalline qualities and magnetic properties

Figure 2(a) shows the out-of-plane XRD and RHEED patterns of the $Mn_{4-x}Ni_xN$ ($x = 0$, 0.1, 0.25, and 0.5) thin films along the STO[100] azimuth, and Fig. 2(b) shows their in-plane XRD patterns. Diffraction peaks of the grown layers appear at small 2θ angles in Fig. 2(a) and overlap with the intense diffraction peaks of the STO substrate because of the excellent lattice match between the $Mn_{4-x}Ni_xN$ films and the STO(001) substrate. Judging by the presence of diffraction peaks such as 002 and 004 from $Mn_{4-x}Ni_xN$, we achieved epitaxial growth of $Mn_{4-x}Ni_xN$ thin films on STO(001) substrates. Very sharp, streaky lines appeared in the RHEED patterns, and Kikuchi lines also verified the highly oriented epitaxial growth of the $Mn_{4-x}Ni_xN$ films. From these sharp peaks and streaks, we conclude that the c-axis of the $Mn_{4-x}Ni_xN$ film is more highly oriented on STO(001) than on MgO(001) owing to better lattice matching. Notably, the diffraction peaks of $Mn_{4-x}Ni_xN$ appear at slightly higher angles than those of cubic STO(001) in Fig. 2(a), showing $c/a < 1$, which indicates the presence of in-plane tensile strain in the grown films. This result agrees with the results obtained for $Mn_{4-x}Ni_xN$ epitaxial thin films on MgO(001).[27] The 002 and 004 diffraction peaks of $Mn_{4-x}Ni_xN$ shift toward a higher angle in Fig. 2(a), which is reasonable, because Ni_4N has a much smaller lattice constant than Mn_4N. However, diffraction peaks other than those belonging to $Mn_{4-x}Ni_xN$ appear at a 2θ value of around 41.3° at $x = 0$ and 0.25 in Fig. 2(b). Tiny but distinct peaks, denoted by arrows, are also observed at $x = 0.1$ and 0.5. We ascribe these peaks to the 200 reflection of MnO formed by interactions with the SiO_2 capping layer.

Figure 3(a) shows the M–H loops of $Mn_{4-x}Ni_xN$ ($x = 0$, .0.1, 0.25, and 0.5) measured by VSM at RT with a magnetic field applied perpendicular to the plane. Table II shows the values of M_S and K_u obtained for $Mn_{4-x}Ni_xN$ films on both STO(001) and MgO(001).[24] The $Mn_{4-x}Ni_xN$ films tend to show a larger M_S on STO(001) than on MgO(001). For example, the M_S of $Mn_{3.9}Ni_{0.1}N$/MgO(001) is 24.2 kA/m, while that of $Mn_{3.9}Ni_{0.1}N$/STO(001) is 47.4 kA/m.

Ni introduction into Mn_4N caused M_S to decrease by 45% at $x = 0.1$ and by 75% at $x = 0.25$. This can be explained using a simple calculation, which is described later. PMA appeared in the $Mn_{3.5}Ni_{0.5}N$ film on STO(001); however, it was absent in the

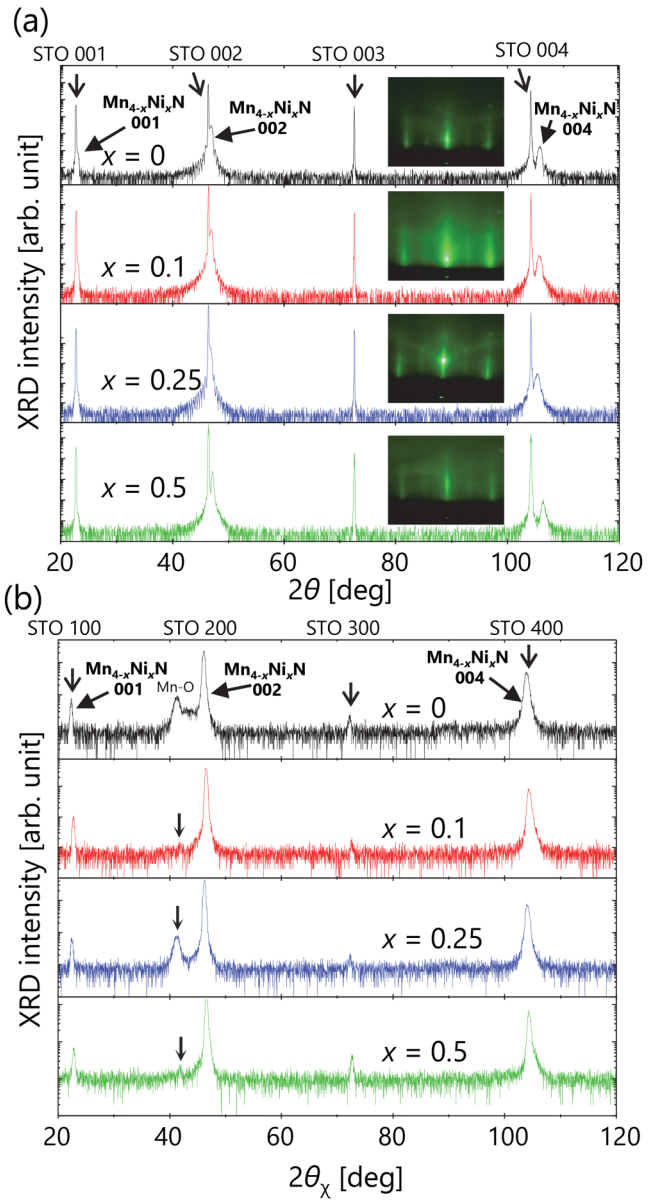

FIG. 2. (a) Out-of-plane XRD (line spectra) and RHEED (inset images) patterns of $Mn_{4-x}Ni_xN$ along the STO[001] azimuth. The arrows indicate the positions of the superlattice diffraction lines. (b) In-plane XRD patterns of $Mn_{4-x}Ni_xN$. The scattering vector was set along the STO[100] azimuth.

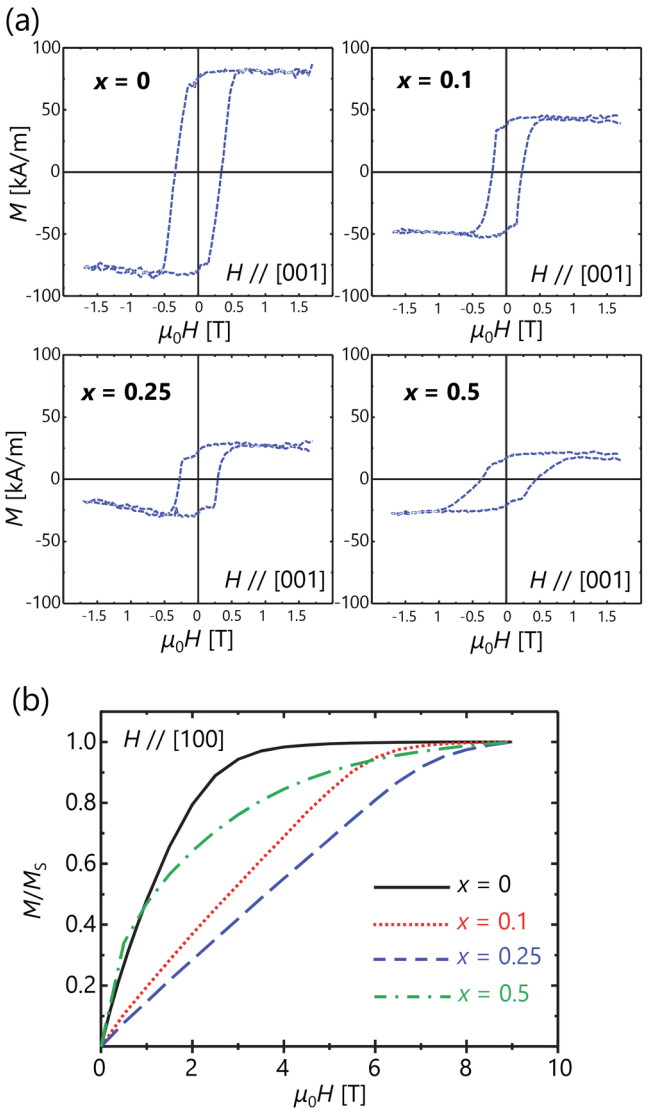

FIG. 3. (a) Magnetization vs magnetic field (M–H) curves of $Mn_{4-x}Ni_xN$ on STO(001) measured at RT by VSM with a magnetic field, H, applied perpendicular to the plane, along the STO[001] azimuth. (b) M/M_S vs magnetic field curves of $Mn_{4-x}Ni_xN$ on STO(001) measured at RT by AHE with H in parallel to the plane, along the STO[100] azimuth.

$Mn_{3.5}Ni_{0.5}N$ film on MgO(001).[27] $Mn_{4-x}Ni_xN$ films on STO(001) showed a larger K_u than on MgO(001) for all x values. In particular, the K_u of $Mn_{3.9}Ni_{0.1}N$ and $Mn_{3.75}Ni_{0.25}N$ films on STO(001) reached values as large as those of Mn_4N films on STO(001). Kinks appeared in the M–H loops of $Mn_{4-x}Ni_xN$ films on STO(001). We attribute this result to mixed phases with hard ($Mn_{4-x}Ni_xN$) and soft magnetism.

TABLE II. $M_S^{STO}(M_S^{MgO})$ and $K_u^{STO}(K_u^{MgO})$ values of $Mn_{4-x}Ni_xN$/STO (MgO)(001).

x	M_S^{STO} (kA/m)	M_S^{MgO} (kA/m)	K_u^{STO} (J/m^3)	K_u^{MgO} (J/m^3)
0	86.6	86.3	1.1×10^5	6.3×10^4
0.1	47.4	24.2	1.4×10^5	2.7×10^4
0.25	30.4	19.0	1.1×10^5	1.0×10^4
0.5	24.4	27.7	4.2×10^4	No anisotropy

Figure 3(b) shows the AHE curves of $Mn_{4-x}Ni_xN$ on STO (001) with a magnetic field applied parallel to the plane along the STO[100] azimuth. A comparison of the M–H curves reveals that a much larger magnetic field was necessary for the magnetization to saturate compared with when the magnetic field was applied normal to the plane, as shown in Fig. 3(a). Based on these results, we can state that $Mn_{4-x}Ni_xN$ films on STO(001) show PMA at $x = 0$, 0.1, 0.25, and 0.5.

B. Magneto-transport properties

In Fig. 4, panels (a) and (b) show the AHE loops of $Mn_{4-x}Ni_xN$ thin films on STO(001) and MgO(001), respectively, with a magnetic field applied perpendicular to the plane. The transverse voltage (V_y) was calculated using Eq. (6),

$$V_y = \left(R_H \frac{B_Z}{t} + \frac{\rho_{AH}}{t}\frac{M_\perp}{M_S}\right) I_x = \frac{\rho_{xy}}{t} I_x, \tag{6}$$

where R_H, B_Z, ρ_{AH}, t, ρ_{xy}, and I_x are the ordinary Hall coefficient, the magnetic flux density perpendicular to the sample surface, the anomalous Hall resistivity, the film thickness, the Hall resistivity, and the current, respectively. We did not consider the planar Hall effect because the anomalous magnetoresistance of the Mn_4N thin film is negligibly small at RT.[25] The slope in the high-H region, where M is saturated, corresponds to the first term in Eq. (5). Thus, we can subtract the contribution of this term from the measured value. Remarkably, the ratio of the remnant magnetization (M_r) to M_S, M_r/M_S, was almost 1 for $x = 0$, 0.1, and 0.25 on STO (001). In contrast, $Mn_{4-x}Ni_xN$ thin films on MgO(001) showed an $M_r/M_S < 1$ and their PMA vanished at $x = 0.5$. Thus, one can speculate that $Mn_{4-x}Ni_xN$ films on STO(001) are preferable for CIDWM applications, because of their sharp magnetization reversal at $x = 0$, 0.1, and 0.25. Conversely, $Mn_{3.5}Ni_{0.5}N$ films on STO(001) and $Mn_{4-x}Ni_xN$ films on MgO(001) showed a slow magnetization reversal, and reversing their magnetization required a large magnetic field. This behavior is caused by the degradation of the crystalline quality of $Mn_{4-x}Ni_xN$ on MgO(001) and $Mn_{3.5}Ni_{0.5}N$ on STO(001), as proven by the fact that the full width at half maximum value obtained from an X-ray ω-scan rocking curve was one order of magnitude larger for the Mn_4N films on MgO(001) than for those on STO(001).[18] In addition, the formation of $Mn_{4-x}Ni_xN$ films becomes more difficult with increasing Ni content x, because the films are significantly decomposed into Ni_8N or Mn–Ni alloys.[27]

Regarding the sign of ρ_{xy} in Figs. 4(a) and 4(b), ρ_{xy} became negative in the $+H$ region for $Mn_{4-x}Ni_xN$ films at $x = 0$ and 0.1. However, the sign of ρ_{xy} was reversed for $Mn_{4-x}Ni_xN$ films between $x = 0.1$ and 0.25, regardless of the substrate. Figure 4(c) shows the dependence of the anomalous Hall angle given by $\theta_{AHE} = \rho_{AH}/\rho_{xx}$, where ρ_{xx} is the longitudinal resistivity of the grown layers with Ni content x. The sign of θ_{AHE} switched from negative to positive between $x = 0.1$ and 0.25, which also indicates magnetic compensation. Such a sudden reversal of θ_{AHE} is probably linked to ferrimagnetic compensation: at the compensation point, the direction of the magnetic moment at each sublattice is reversed with respect to the external magnetic field. Below the compensation point ($x = 0$ and 0.1), the magnetic moment at the Mn(I) sites

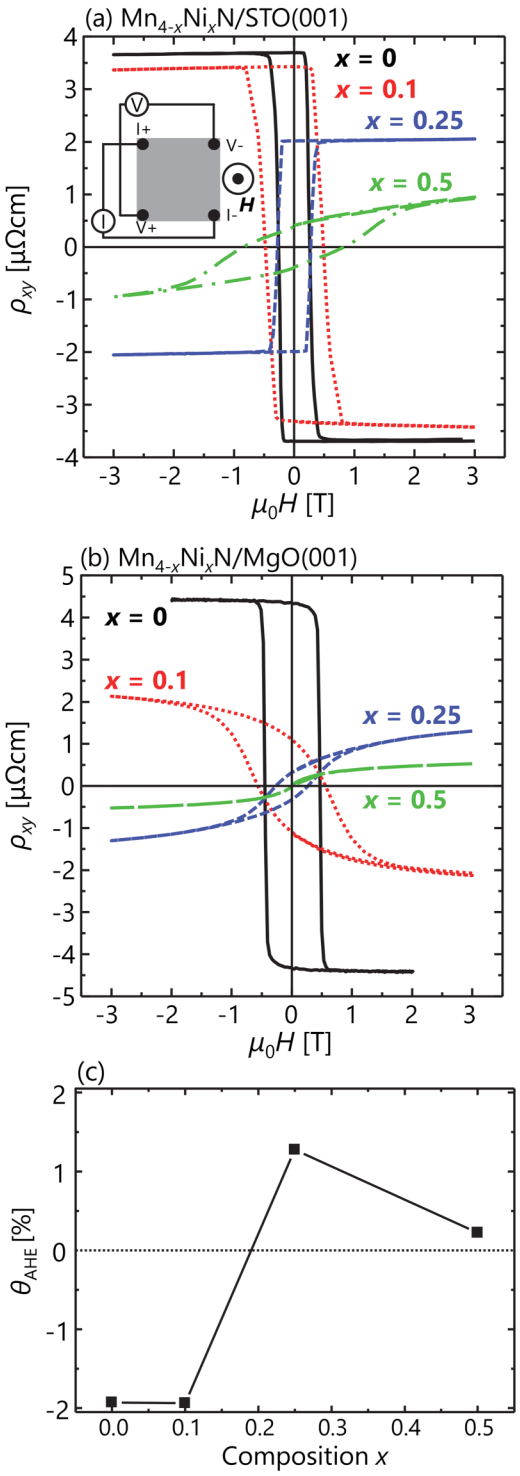

FIG. 4. Anomalous Hall effect measured at RT for $Mn_{4-x}Ni_xN$ thin films on (a) STO(001) and (b) MgO(001) substrates. A magnetic field, H, was applied perpendicular to the plane. (c) Ni content x dependence of θ_{AHE} measured at RT.

determines the direction of the magnetization, while above the compensation point ($x = 0.25$), the direction of the magnetization is determined by the magnetic moment at the Mn(II) sites. Therefore, this sign reversal is commonly used to confirm the compensation point in rare-earth ferrimagnets.[11,40] It should be noted that a reversal of the sign of ρ_{AH} is common in alloys with various compositions, for example, in Mn_4N-based materials. Isogami *et al.* recently investigated the magneto-transport properties of $Mn_{4-x}Fe_xN$ thin films[41] and found that the sign of ρ_{AH} reversed at around $x = 1$. However, the ρ_{AH} changed gradually with x at 300 K because of the shift of the Fermi level E_F and because of the change in the exchange coupling splitting energy[42] caused by Fe doping. Meng *et al.* also reported a reversal of the sign of ρ_{AH} in $Mn_{4-x}Dy_xN$ thin films for $x = 0.08$ and 0.2[43] and concluded that this was caused by changes to the band structure and position of the E_F. In the $Mn_{4-x}Ni_xN$ system, the sign reversal was caused by substitution with a small amount of Ni, and the change in the sign of ρ_{AH} was quite sharp when the Ni content was varied, which differs from the smooth change observed for $Mn_{4-x}Fe_xN$ thin films. Therefore, we expect that this reversal is caused by the compensation point being crossed by the change in the composition.

C. Discussion on compensation

Figure 5 shows the temperature dependence of M_S, $M_S(T)$, for $Mn_{4-x}Ni_xN$ films at $x = 0$, 0.1, and 0.25 normalized using the M_S at RT, $M_{S,\,RT}$. For comparison, the temperature dependences of M_S for $Gd_{21}(FeCo)_{79}$ and $Gd_{23}(FeCo)_{77}$ are inserted in Fig. 5.[44] The curve for $Gd_{21}(FeCo)_{79}$ shows that the behavior of FeCo is dominant at all temperatures, whereas a transition from FeCo- to Gd-dominant is observed for $Gd_{23}(FeCo)_{77}$, i.e., with decreasing temperature, Gd dominates owing to its larger magnetic moment. In contrast, as the temperature increases for $Gd_{23}(FeCo)_{77}$, the net magnetization, m_{net}, decreases and eventually vanishes at $T_M = 75$ K, because the demagnetization process is faster in Gd. As the temperature decreases for $Mn_{4-x}Ni_xN$ films, M_S increased for $x = 0$ and 0.1 and decreased for $x = 0.25$. Mekata confirmed similar temperature dependences of the magnetization in Sn- and In-doped Mn_4N when magnetic compensation occurred.[45] Thus, we propose that in $Mn_{4-x}Ni_xN$, different sublattices have different temperature dependences of the magnetization owing to 3d metals at the I sites being farther away from the N atoms at the body-centered site than those at the II sites. Thus, 3d metal atoms at I sites tend to be localized. In contrast, 3d metals located at II sites are closer to N atoms and thus tend to be itinerant.[46]

Because of the sharp decrease in M_S with increasing x [cf. Fig. 3(a)], the sign reversal of ρ_{xy} and θ_{AHE} in Figs. 4(a)–4(c), and the difference in the temperature dependence of the magnetization depending on the Ni content x (cf. Fig. 5), we believe that the magnetization of $Mn_{4-x}Ni_xN$ might be compensated by a small amount of Ni. Let us discuss this possibility, assuming the following two hypotheses. Firstly, Ni atoms are positioned at I sites. This hypothesis is based on the fact that Ni atoms in $Fe_{4-x}Ni_xN$ preferentially occupy I sites according to X-ray magnetic circular dichroism data.[47] As mentioned above, the M_S of Mn_4N drastically decreased with a small amount of Ni substitution, and the magnetic moment of Mn atoms is larger at I sites than at II sites. Thus, Ni atoms

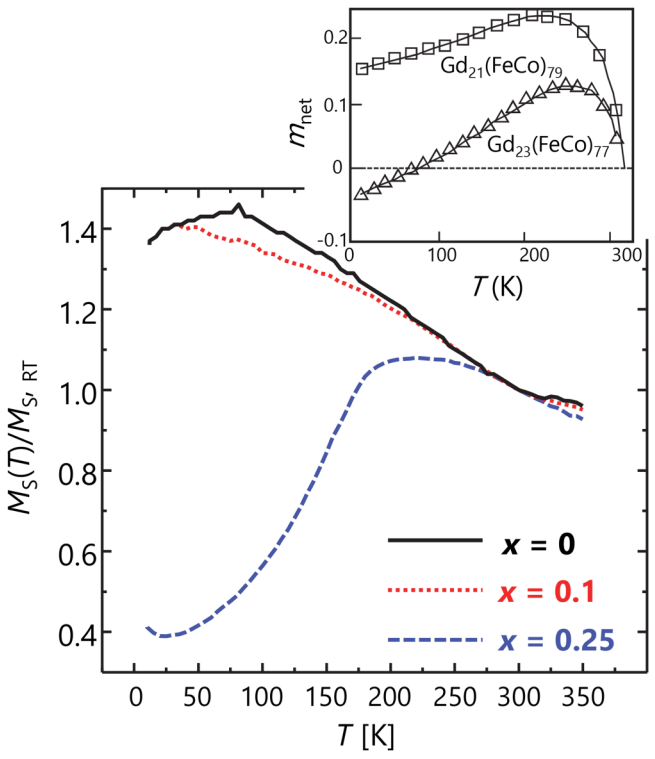

FIG. 5. Temperature dependence of the magnetization of $Mn_{4-x}Ni_xN$ films ($x = 0$, 0.1, and 0.25). Samples were measured under field cooling, and the magnetic field, H, was applied perpendicular to the plane. The inset is reprinted with permission from Zhu *et al.*, J. Appl. Phys. **124**, 193901 (2018). Copyright 2018 AIP Publishing LLC.

preferentially occupying I sites is necessary to explain the magnetization compensation in $Mn_{4-x}Ni_xN$. Secondly, the magnetic moment of a Ni atom is assumed to be 0.6 μ_B based on a report on the calculation of magnetic moments of Ni atoms in Ni_4N[35] and on the Slater–Pauling curve.[48] Concerning the direction of the magnetic moment of the Ni atoms at the I sites, Ni(I), there are two options: the magnetic moment can be parallel to that of Mn(I) or Mn(II). When we assume the direction of the magnetic moment of Mn(I) to be positive, the parallel and antiparallel magnetic moments ($\mu_\uparrow$ and $\mu_\downarrow$) in a unit cell are given by Eqs. (7) and (8), respectively, when the magnetic moment of Ni is parallel to that of Mn(I),

$$\mu_\uparrow = (1-x)\mu^\uparrow_{Mn(I)} + x\mu^\uparrow_{Ni(I)}, \tag{7}$$

$$\mu_\downarrow = 3\mu^\downarrow_{Mn(II)}. \tag{8}$$

Here, $\mu^\uparrow_{Mn(I)}$, $\mu^\downarrow_{Mn(II)}$, and $\mu^\uparrow_{Ni(I)}$ are the magnetic moments of Mn(I), Mn(II), and Ni(I) atoms, respectively. Thus, the net magnetic moment (μ_{net}) per unit cell can be described by

$$\mu_{net} = (1-x)\mu^\uparrow_{Mn(I)} + x\mu^\uparrow_{Ni(I)} + 3\mu^\downarrow_{Mn(II)}. \tag{9}$$

TABLE III. Calculated contributions of Mn(I), Mn(II), and Ni(I) atoms to the magnetic moment and measured magnetizations.

x	$(1-x)\mu_I^{Mn\uparrow}$ (μ_B)	$x\mu_I^{Ni\uparrow}$ (μ_B)	$x\mu_I^{Ni\downarrow}$ (μ_B)	$3\mu_{II}^{Mn\downarrow}$ (μ_B)	$\mu_\uparrow$ (μ_B)	$\mu_\downarrow$ (μ_B)	μ_{net} (μ_B)	M_S^{cal} (kA/m)	M_S^{exp} (kA/m)
0	3.53	…	…	−2.67	3.53	−2.67	0.86	136.9	86.6
0.1	3.18	0.06	…		3.24	−2.67	0.57	90.3	47.4
		…	−0.06		3.18	−2.73	0.45	71.2	
0.25	2.65	0.15	…		2.80	−2.67	0.13	20.3	30.4
		…	−0.15		2.65	−2.82	−0.17	−27.5	
0.5	1.77	0.30	…		2.07	−2.67	−0.60	−96.4	24.4
		…	−0.30		1.77	−2.97	−1.20	−191.8	

Similarly, when the magnetic moment of Ni(I) is parallel to that of Mn(II), the net magnetic moment per unit cell can be described as Eq. (10) using the magnetic moment of Ni atoms $\mu_{Ni(I)}^{\downarrow}$,

$$\mu_{net} = (1-x)\mu_{Mn(I)}^{\uparrow} + x\mu_{Ni(I)}^{\downarrow} + 3\mu_{Mn(II)}^{\downarrow}. \quad (10)$$

Table III shows the contribution to the magnetic moment per unit cell from Mn(I), Mn(II), and Ni(I) atoms and the calculated M_S. For comparison, the measured $M_S(M_S^{exp})$ and calculated (M_S^{cal}) values are also shown.

Our simple model explains the experimental results quite well. Most importantly, it shows that the magnetization of $Mn_{4-x}Ni_xN$ becomes zero at small x regardless of the direction of the magnetic moment of Ni(I). The calculated compensation composition of Ni atoms is $x = 0.29$ for $\mu_{Ni(I)}^{\uparrow} // \mu_{Mn(I)}^{\uparrow}$ and $x = 0.21$ for $\mu_{Ni(I)}^{\downarrow} // \mu_{Mn(II)}^{\downarrow}$. There is, however, a large difference in M_S between the calculation and the experiment at $x = 0.5$, as shown in Fig. 6. We cannot exclude the possibility that Ni atoms would begin to occupy II sites as x increases. In this regard, X-ray magnetic circular dichroism could be a powerful tool to determine the site of Ni atoms in $Mn_{4-x}Ni_xN$. Additionally, we must correctly evaluate the composition, i.e., the value of x, in $Mn_{4-x}Ni_xN$ films at which magnetic compensation occurs. Rutherford back-scattering spectrometry, energy-dispersive X-ray spectrometry, or inductively-coupled plasma mass spectrometry could be used for this purpose.

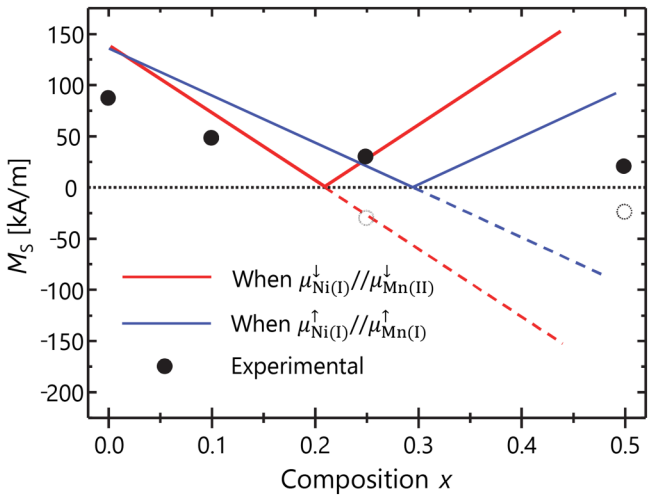

FIG. 6. Calculated and measured Ni content x dependence of M_S.

IV. CONCLUSION

We grew highly c-axis-oriented epitaxial $Mn_{4-x}Ni_xN$ ($x = 0$, 0.1, 0.25, and 0.5) thin films by MBE on STO(001) substrates and measured their magnetic and magneto-transport properties, which we compared with those of $Mn_{4-x}Ni_xN$ films on MgO(001) substrates. The $Mn_{4-x}Ni_xN$ thin films on STO(001) showed a squareness ratio of $M_r/M_S = 1$, fast magnetization reversal, and a perpendicular magnetization when $x \leq 0.25$, which are desirable features for CIDWM devices. In contrast, the $Mn_{4-x}Ni_xN$ thin films on MgO (001) substrates did not show such features. We ascribed this difference to the superior crystalline qualities of $Mn_{4-x}Ni_xN$ thin films on STO(001) owing to the smaller lattice mismatch compared with $Mn_{4-x}Ni_xN$ thin films on MgO(001). Three factors point toward magnetic compensation in $Mn_{4-x}Ni_xN$ occurring between $x = 0.1$ and 0.25: the sharp decrease in M_S when increasing the Ni content, the sign reversal of the anomalous Hall effect, and the anomalous temperature dependence of M_S. We discussed the validity of this assumption by taking into account that the Ni atoms preferentially occupy I sites and that the magnetic moment of Ni atoms is $0.6\,\mu_B$. We conclude that magnetic compensation is likely to occur regardless of the direction of the magnetic moment of the Ni atoms at the I sites. We thus believe that, in view of its magnetic properties, $Mn_{4-x}Ni_xN$ close to the compensation composition is a very attractive candidate for applications based on spin transfer torques or spin–orbit torques, particularly for CIDWM.

ACKNOWLEDGMENTS

The samples' magnetic properties were measured with the help of Professor H. Yanagihara of the University of Tsukuba. The anomalous Hall effect measurements using a physical properties measurement system were performed with the help of Associate Professor T. Koyano of the Cryogenics Division of the University of Tsukuba. The authors would like to express their sincere thanks to Dr. S. Mitani of the National Institute for Materials Science in Japan for his helpful discussions. This work received support from the MEXT in Japan and the French ANR program through projects OISO (No. ANR-17-CE24-0026-03), TOPRISE (No. ANR-16-CE24-0017), IDEX ISP DOMINO, and the Laboratoire d'Excellence LANEF (No. ANR-10-LABX-51-01).

REFERENCES

[1]L. Berger, J. Appl. Phys. **49**, 2156 (1978).
[2]J. C. Slonczewski, J. Magn. Magn. Mater. **159**, L1 (1996).
[3]I. M. Miron, K. Garello, G. Gaudin, P. J. Zermatten, M. V. Costache, S. Auffret, S. Bandiera, B. Rodmacq, A. Schuhl, and P. Gambardella, Nature **476**, 189 (2011).
[4]L. Liu, C. F. Pai, Y. Li, H. W. Tseng, D. C. Ralph, and R. A. Buhrman, Science **336**, 555 (2012).
[5]S. Parkin, M. Hayashi, and L. Thomas, Science **320**, 190 (2008).
[6]S. Parkin and S. H. Yang, Nat. Nanotechnol. **10**, 195 (2015).
[7]S. Fukami *et al.*, VLSI Tech. Symp. Dig. Tech. Pap. (2009). p. 230.
[8]C. O. Avci, E. R. Baumgartner, L. Beran, A. Quindeau, P. Gambardella, C. A. Ross, and G. S. D. Beach, Appl. Phys. Lett. **111**, 072406 (2017).
[9]S.-H. Yang, K.-S. Ryu, and S. Parkin, Nat. Nanotechnol. **10**, 221 (2015).
[10]T. Komine, K. Takahashi, A. Ooba, and R. Sugita, J. Appl. Phys. **109**, 07D503 (2011).
[11]K.-J. Kim, S. K. Kim, Y. Hirata, S.-H. Oh, T. Tono, D.-H. Kim, T. Okuno, W. S. Ham, S. Kim, G. Go, Y. Tserkovnyak, A. Tsukamoto, T. Moriyama, K.-J. Lee, and T. Ono, Nat. Mater. **16**, 1187 (2017).
[12]K. Ueda, M. Mann, P. W. P. de Brouwer, D. Bono, and G. S. D. Beach, Phys. Rev. B **96**, 064410 (2017).
[13]M. Imai, Y. Ogata, H. Chudo, M. Ono, K. Harii, M. Matsuno, Y. Ohnuma, S. Maekawa, and E. Saitoh, Appl. Phys. Lett. **113**, 052402 (2018).
[14]L. Caretta, M. Mann, F. Büttner, K. Ueda, B. Pfau, C. M. Günther, P. Hessing, A. Churikova, C. Klose, M. Schneider, D. Engel, C. Marcus, D. Bono, K. Bagschik, S. Eisebitt, and G. S. D. Beach, Nat. Nanotechnol. **13**, 1154 (2018).
[15]S.-H. Ph, S. K. Kim, D.-K. Lee, G. Go, K.-J. Kim, T. Ono, Y. Tserkovnyak, and K.-J. Lee, Phys. Rev. B **96**, 100407(R) (2017).
[16]D. Lau, J. P. Pellegren, H. T. Nembach, J. M. Shaw, and V. Sokalski, Phys. Rev. B **97**, 184410 (2018).
[17]R. Bläsing, T. Ma, S.-H. Yang, C. Garg, F. K. Dejene, A. T. N'Diaye, G. Chen, K. Liu, and S. S. P. Parkin, Nat. Commun. **9**, 4984 (2018).
[18]T. Gushi, L. Vila, O. Fruchart, A. Marty, S. Pizzini, J. Vogel, F. Takata, A. Anzai, K. Toko, T. Suemasu, and J.-P. Attané, Jpn. J. Appl. Phys. **57**, 120310 (2018).
[19]T. Gushi, M. Klug, J. Pena Garcia, J.P. Attané, J. Vogel, T. Suemasu, S. Pizzini, and L. Vila, e-print arXiv:1901.06868.
[20]W. J. Takei, R. R. Heikes, and G. Shirane, Phys. Rev. **125**, 1893 (1962).
[21]C. Li, Y. Yang, L. Lv, H. Huang, Z. Wang, and S. Yang, J. Alloys. Compd. **457**, 57 (2008).
[22]Y. Yasutomi, K. Ito, T. Sanai, K. Toko, and T. Suemasu, J. Appl. Phys. **115**, 17A935 (2014).
[23]K. Ito, Y. Yasutomi, K. Kabara, T. Gushi, S. Higashikozono, K. Toko, M. Tsunoda, and T. Suemasu, AIP Adv. **6**, 056201 (2016).
[24]X. Shen, A. Chikamatsu, K. Shigematsu, Y. Hirose, T. Fukumura, and T. Hasegawa, Appl. Phys. Lett. **105**, 072410 (2014).
[25]K. Kabara and M. Tsunoda, J. Appl. Phys. **117**, 17B512 (2015).
[26]A. Anzai, F. Takata, T. Gushi, K. Toko, and T. Suemasu, J. Cryst. Growth **489**, 20 (2018).
[27]T. Komori, A. Anzai, T. Gushi, K. Toko, and T. Suemasu, J. Cryst. Growth **507**, 163 (2019).
[28]S. Emori and G. S. D. Beach, Appl. Phys. Lett. **98**, 132508 (2011).
[29]A. Thiaville, J. M. García, and J. Miltat, J. Magn. Magn. Mater. **242–245**, 1061 (2002).
[30]A. Mougin, M. Cormier, J. P. Adam, P. J. Metaxas, and J. Ferré, Europhys. Lett. **78**, 57007 (2007).
[31]A. Thiaville, Y. Nakatani, J. Miltat, and Y. Suzuki, Europhys. Lett. **69**, 990 (2005).
[32]K. M. Ching, W. D. Chang, and T. S. Chin, J. Alloys Compd. **222**, 184 (1995).
[33]K. M. Ching, W. D. Chang, T. S. Chin, J. G. Duh, and H. C. Ku, J. Appl. Phys. **76**, 6582 (1998).
[34]K. Kabara and M. Tsunoda, AIP Adv. **7**, 056416 (2017).
[35]M. Meng, S. X. Wu, L. Z. Ren, W. Q. Zhou, Y. J. Wang, G. L. Wang, and S. W. Li, Appl. Phys. Lett. **106**, 032407 (2015).
[36]F. Takata, K. Ito, S. Higashikozono, T. Gushi, K. Toko, and T. Suemasu, J. Appl. Phys. **120**, 083907 (2016).
[37]M. Kawasaki, K. Takahashi, T. Maeda, R. Tsuchiya, M. Shinohara, O. Ishiyama, T. Yonezawa, M. Yoshimoto, and H. Koinume, Science **266**, 1540 (1994).
[38]D. Ravelosona, A. Cebollada, F. Briones, C. Diaz-Paniagua, M. A. Hidalgo, and F. Batallan, Phys. Rev. B **59**, 4322 (1999).
[39]K. Yamada, H. Kakizaki, K. Shimamura, M. Kawaguchi, S. Fukami, N. Ishiwata, D. Chiba, and T. Ono, Appl. Phys. Express **6**, 073004 (2013).
[40]Y. Hirata, D. H. Kim, T. Ohno, T. Nishimura, D. Y. Kim, Y. Futakawa, H. Yoshikawa, A. Tsukamoto, K. J. Kim, S. B. Choe, and T. Ono, Phys. Rev. B **97**, 220403(R) (2018).
[41]S. Isogami, A. Anzai, T. Gushi, T. Komori, and T. Suemasu, Jpn. J. Appl. Phys. **57**, 120305 (2018).
[42]L. Chen, J. Appl. Phys. **100**, 113717 (2006).
[43]M. Meng, S. X. Wu, W. Q. Zhou, L. Z. Ren, Y. J. Wang, G. L. Wang, and S. W. Li, J. Appl. Phys. **118**, 053911 (2015).
[44]Z. Zhu, X. Fong, and G. Liang, J. Appl. Phys. **124**, 193901 (2018).
[45]M. Mekata, J. Phys. Soc. Jpn. **17**, 5 (1962).
[46]X. G. Ma, J. J. Jiang, P. Liang, J. Wang, Q. Ma, and Q. K. Zhang, J. Alloys. Compd. **480**, 475 (2009).
[47]F. Takata, K. Ito, Y. Takada, Y. Saitoh, K. Takahashi, A. Kimura, and T. Suemasu, Phys. Rev. Mater. **2**, 024407 (2018).
[48]C. Takahashi, M. Ogura, and H. Araki, J. Phys. Condens. Matter **19**, 365233 (2007).